Radiative Transfer Solutions for Purely Absorbing Gray and Nongray Gases Within a Cubical Enclosure

Tae-Kuk Kim*
Department of Mechanical Engineering, Chung-Ang University
Won-Hee Park, Chang-Hyung Lee
Graduate student, Chung-Ang University

Although there are many different solution schemes proposed for multidimensional radiative transfer, reference solutions to benchmark these methods are very rare in the literature. In this paper we produced some accurate solutions for purely absorbing gray and nongray gases including H_2O and CO_2 by using the discrete transfer method with sufficiently accurate T_{95} quadrature set. The spectral transmittances of the mixtures of H_2O and CO_2 are estimated by using the narrow band model. The gray gas solutions are obtained for different absorption coefficients, and the nongray real gas solutions are obtained for different mixture fractions of H_2O and CO_2. The numerical solutions presented in this paper are proved to be sufficiently accurate as compared to the available exact solutions and they may be used as reference solutions in evaluating various solution schemes.

Key Words : Radiation, Narrow Band Model, Nongray Gas, Benchmark Solution, T_N Quadrature, Ray Tracing Method

Nomenclature

a : Absorption coefficient, m^{-1}
F : Blackbody fraction
G : Average intensity, $W/(m^2 \cdot sr)$
G^* : Dimensionless average intensity $(=\pi G/(\sigma T^4_{hot}))$
I_λ : Spectral radiative intensity $W/(m^2 \cdot \mu m \cdot sr)$
L : System dimension, m
m : Index of the discrete direction
M : Total number of the discrete directions $(=8N^2$ for T_N quadrature)
$\hat{n}$: Unit vector normal to the wall
N : Order of the quadrature
q_w : Net radiative wall heat flux, W/m^2
q_w^* : Dimensionless net radiative wall heat flux $(=q_w/(\sigma T^*_{hot}))$
s : Location, m
S_λ : Spectral radiative source function $W/(m^2 \cdot \mu m \cdot sr)$
T : Absolute temperature, K
x, y, z : Coordinates, m
x^* : Dimensionless x coordinate $(=x/L)$
y^* : Dimensionless y coordinate $(=y/L)$
z^* : Dimensionless z coordinate $(=z/L)$
w_m : Angular weight for m^{th} discrete direction

Greeks

β : Extinction coefficient, m^{-1}
μ, ξ, η : Direction cosines
$\Delta\lambda_k$: Width of the k^{th} band
Δs_m : Distance of the ray in m^{th} discrete direction
Φ : Scattering phase function
σ : Stefan-Boltzmann constant $W/(\mu m \cdot K^4)$
σ_s : Scattering coefficient, m^{-1}
τ : Transmittance
Ω : Direction

* Corresponding Author,
E-mail : kimtk@cau.ac.kr
TEL : +82-2-820-5282; **FAX** : +82-2-814-9476
Department of Mechanical Engineering, Chung-Ang University, #221, Huksuk-dong, Dongjak-ku, Seoul 156-756, Korea.(Manuscript **Received** October 2, 2000 ; **Revised** February 15, 2001)

Subscripts

b	: Blackbody
$cold$	: Cold wall
$exact$	: Exact solution
g	: gas
hot	: Hot wall
k	: k^{th} band
L	: Lower limit of the band
p	: Estimation point
$side$	: Side wall
u	: Upstream point
U	: Upper limit of the band
w	: Wall
λ	: Spectral

Subscripts

*	: Dimensionless
-	: Band average

1. Introduction

Modeling of the radiative transfer within multi-dimensional enclosures filled with participating media are frequently required for design of various energy systems such as combustors, industrial furnaces, boilers etc. Various modeling schemes are available and under development for this purpose. Among them the zonal method (Hottel, 1967), the Monte Carlo method (Howell and Perlmutter, 1964), the PN method (Menguc and Viskanta, 1985), the flux method (Lockwood and Spalding, 1971) and the SN discrete ordinates method (DOM) (Carlson and Lathrop, 1968; Fiveland, 1984; Kim and Lee, 1988) are suggested for enclosures of regular shapes, while the finite volume method (FVM) (Raithby and Chui, 1990; Chai, Lee and Patankar, 1994) and the discrete ordinates interpolation method (DOIM) (Cheong and Song, 1997; Seo and Kim, 1998; Kim, Seo, Min and Son, 1998) are suggested for enclosures of irregular shapes.

For gray gases in two dimensional system, Siegel(1991) obtained analytical solutions. An extension for a nongray medium is by Siegel (1992). Cha and Song(1999) compare their numerical result with analytical heat fluxes in isothermal gray medium. Although there are many solution methods suggested for multi-dimensional systems, the applicabilities and accuracies of these methods have not yet been fully tested especially for nongray gases. This is because the measured data and/or the benchmark solutions for the multi-dimensional nongray gas radiation are very rare in the literature. Until now most of the nongray radiative transfer solutions are reported for one-dimensional planar slabs with uniform and non-uniform temperature and concentration profiles (Grosshandler, 1980; Zhang, Soufiani, and Taine, 1988; Soufiani and Taine, 1989; Kim, Menart and Lee, 1991).

In this paper we present some benchmark radiative transfer solutions for a black walled cubical system filled with purely absorbing gray and nongray gases where the medium is assumed to be uniform in properties and temperature. The solution method used is the discrete transfer method by Lockwood and Shsh (1981), which is applied by tracing the rays starting from the black walls to the point in the medium and/or on the black wall. The discrete transfer method is applied by using the T_N quadrature set (Thurgood, Pollard and Becker, 1995) where the T_{95} quadrature set(total 72,200 directions for every node point) for angular integrations are considered. The nongray gas effects by the H_2O and CO_2 gases are studied by using the narrow band model and the narrow band data from the RADCAL (Grosshandler, 1980) are used for the computations of the transmittances. Although the solution method used in this study is not suitable for engineering purposes, the resulting solutions are proved to be quite accurate and can be regarded as the benchmark solutions.

2. Radiative Transfer Equation(RTE)

The integral form of the spectral radiative transfer equation (RTE) along a line of travel s in Ω direction can be written as (Siegel and Howell, 1992; Modest, 1993)

$$I_{\lambda,p}(s_p,\Omega)=I_{\lambda,u}(s_u,\Omega)e^{-\int_{s_u}^{s_p}\beta_\lambda(s)ds}$$

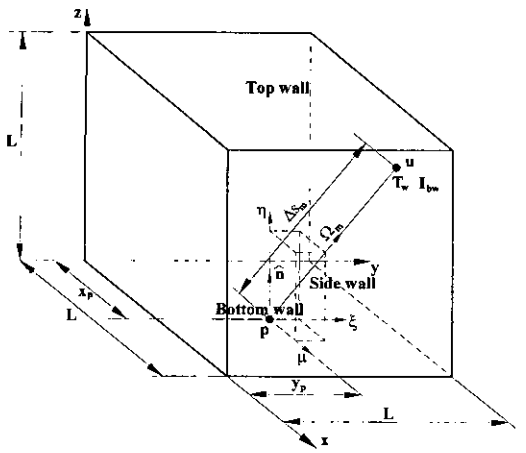

Fig. 1 Schematic drawing of the cubical enclosure

$$+\int_{s_u}^{s_p} S_\lambda(s, \Omega) e^{-\int_s^{s_p} \beta_\lambda(s')ds'} ds \quad (1)$$

And the radiative source function is expressed as

$$S_\lambda(s, \Omega)=a_\lambda(s)I_{\lambda b}(s)+\frac{\sigma_{s\lambda}(s)}{4\pi} \cdot \int_{4\pi} I_\lambda(s, \Omega')\Phi_\lambda(\Omega ; \Omega')d\Omega' \quad (2)$$

where, a_γ and $\sigma_{s\lambda}$ are the absorption and the scattering coefficients of the medium and are related to the extinction coefficient as $\beta_\lambda=a_\lambda+\sigma_{s\lambda}$. Φ is the scattering phase function, and $I_{\lambda b}$ is the blackbody intensity of the medium at s.

For purely absorbing uniform media ($\sigma_{s\lambda}=0_\lambda=constant$, $T_g=constant$) within a black walled enclosure, the RTE can be expressed in a simplified form as

$$I_{\lambda,p}(s_p, \Omega)=I_{\lambda,u}(s_u, \Omega)e^{-(s_p-s_u)a_\lambda} + \int_{s_u}^{s_p} [a_\lambda I_{\lambda b}] e^{-(s_p-s)a_\lambda} ds \quad (3)$$

where the estimation point $s_p=(x_p, y_p, z_p)$ can be located on a wall or in the medium but the upstream point $s_u=(x_u, y_u, z_u)$, where the ray starts, is located on a wall to trace a radiative ray as shown in Fig. 1.

Since the medium considered is uniform in temperature and properties, the integrand in the parenthesis in Eq. (3) is independent of the location s. After performing integration, Eq. (3) can be rearranged in a following form.

$$I_{\lambda,\,p}(s_p, \Omega)=I_{\lambda b}+[I_{\lambda,\,u}(s_u, \Omega)-I_{\lambda b}]e^{-(s_p-s_u)a_\lambda} \quad (4)$$

Where $I_{\lambda b}$ is the black body intensity of the gas medium at wavelength λ and temperature T_g.

For purely absorbing uniform media, the solution procedure by using Eq. (4) is effectively decoupled from the local effects and angular dependencies. Therefore, we may obtain the solutions by Eq. (4) only at designated points, by which the computational efforts are dramatically reduced to allow a high order angular discretization and to apply an accurate narrow band approximation. In this paper, the radiative heat fluxes are computed on the bottom and top walls along the x axis at $y=0.5L$ and on the side wall along the z axis at $y=0.5L$, respectively. And the average intensities are computed along the z axis through the medium at $x=y=0.5L$. These net radiative heat fluxes and the average intensities are then computed for both gray and nongray gases.

3. Numerical Solutions

By using Eq. (4) under various conditions, the radiative intensity solutions are obtained by tracing the rays originated from the black walls as illustrated in Fig. 1. These rays are considered for each discrete direction Ω_m, where $m=1, \cdots, M$, at every estimation point s_p. The discrete directions are set according to the T_{95} quadrature set with $M=72200$. The cubical enclosure considered has the dimensions of $L\times L\times L$ with $L=1m$.

3.1 Gray gas solutions

For gray gases, Eq. (4) is used without subscript λ. The radiative intensity at a point p on a wall or in the medium can be determined by using Eq. (4) for a discrete direction $\Omega_m=(\mu, \xi, \eta)_m$ as

$$I_{p,m}=I_b+(I_{u,m}-I_b)e^{-\Delta s_m a} \quad (5)$$

where $m=1, 2, \cdots, M$, $I_{p,m}$ and $I_{p,m}$ are the radiative intensities in the m^{th} discrete direction at points p and u, respectively. The path length Δs_m is the distance between the two points, p and u, as shown in Fig. 1. And $I_b=\sigma T_g^4/\pi$ is the blackbody intensity of the medium.

If the upstream point u is on a black surface at

T_w, then $I_{u,m}=I_{bw}=\sigma T_w^4/\pi$ and Eq. (5) becomes

$$I_{p,m}=I_b+(I_{bw}-I_b)e^{-\Delta s_m a} \tag{6}$$

The radiative intensities obtained from Eq. (6) are then used to compute the radiative wall heat flux q_w in the z direction and the average intensity G by using an integral quadrature as

$$q_w^*=\frac{q_w}{\sigma T_{hot}^4}=\frac{1}{\sigma T_{hot}^4}\sum_{m=1}^{M} I_{p,m}\eta_m w_m \tag{7}$$

$$G^*=\frac{\pi G}{\sigma T_{hot}^4}=\frac{1}{4\sigma T_{hot}^4}\sum_{m=1}^{M} I_{p,m} w_m \tag{8}$$

The w_m and η_m are the quadrature weight and the direction cosine for the m^{th} ordinate direction which form the T_{95} quadrature set. The gray gas solution obtained by this method is well matched with the published data in the literature(Cha and Song, 1999)

3.1.1 Simple gray gas system

As an ultimate case, if the bottom black wall is maintained at $T_{hot}=1000K$ and all the other black walls and the medium are maintained cold at $T_g=T_{cold}=0.5T_{hot}$, the radiative intensity for all incident directions into the bottom wall is simply $I_{p,m}=\sigma T^4{}_{cold}/\pi$ for $|\Omega_m\cdot\hat{n}|<0$ by examining Eq. (6). The radiative intensity emitted from the black hot wall is $I_{p,m}=\sigma T_{hot}^4/\pi$ for $|\Omega_m\cdot\hat{n}|>0$. Therefore, the exact net radiative heat flux from the hot wall can be obtained as

$$q_{w,hot}=\int_{4\pi} I_p\eta d\Omega=\sigma(T_{hot}^4-T_{cold}^4) \tag{9}$$

or in a dimensionless form as

$$q^*{}_{w.hot}=\frac{q_{w,hot}}{\sigma T_{hot}^4}=1-\left(\frac{T_{cold}}{T_{hot}}\right)^4 \tag{10}$$

Similarly, the exact average intensity on the hot wall can also be obtained as

$$G_{w.hot}=\frac{1}{4\pi}\int_{4\pi} I_p d\Omega=\frac{\sigma}{2\pi}(T_{hot}^4+T_{cold}^4) \tag{11}$$

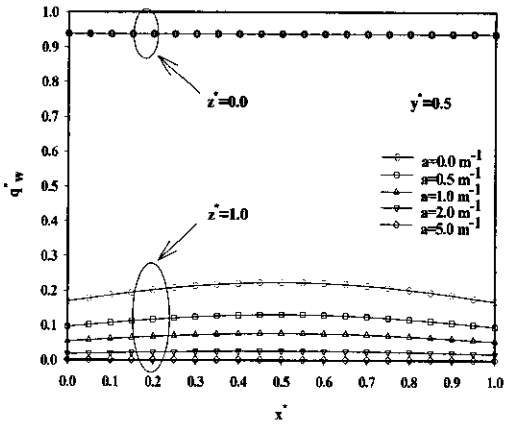

Fig. 2 Net wall heat fluxes for gray gases($T_g=0.5$ T_{hot})

or in a dimensionless form as

$$G_{w,hot}^*=\frac{\pi G_{w,hot}}{\sigma T_{hot}^4}=\frac{1}{2}\left[1+\left(\frac{T_{cold}}{T_{hot}}\right)^4\right] \tag{12}$$

Therefore, for $T_{cold}/T_{hot}=0.5$, the exact dimensionless hot wall radiative heat flux is $(q_{w,hot}^*)_{exact}=0.9375$ and the exact dimensionless hot wall average intensity is $(G_{w,hot}^*)_{exact}=0.53125$.

The comprehensive numerical tests say that the results obtained using the T_{10} quadrature set is comparable to those obtained using the level symmetric S_{10} quadrature set (Carlson and Lathrop, 1968) where the highest order is usually limited to S_{16} due to negative angular weights. However, for the problem considered here, the ray effect is appreciable by overshooting the solution limits even with the T_{50} quadrature set. We decided to use the T_{95} quadrature set with double precision, which showed no visible ray effects, for the numerical solutions presented throughout this paper. The typical c.p.u. time spent for the gray gas solution by using the T_{95} quadrature set is about 1.2 hours on a Pentium II 400MHz PC.

The T_{95} solution results in the constant dimensionless net hot wall heat flux of 0.937502 as shown in Fig. 2 which is quite accurate with a percent relative error of 0.000213% as compared to the exact solution of 0.9375. Figure 2 also

Table 1 Net hot and cold wall heat fluxes(T_g=0.5 T_{hot})

x^*	a=0.0		a=0.5		a=1.0		a=2.0		a=5.0	
	$q^*_{w,hot}$	$q^*_{w,cold}$	$q^*_{w,hot}$	$q^*_{w,cold}$	$q^*_{w,hot}$	$q^*_{w,cold}$	$q^*_{w,hot}$	$q^*_{w,cold}$	$q^*_{w,hot}$	$q^*_{w,cold}$
0.00	9.37502E-01	1.69549E-01	9.37502E-01	9.62003E-02	9.37502E-01	5.47449E-02	9.37502E-01	1.78750E-02	9.37502E-01	6.57274E-04
0.05	9.37502E-01	1.77908E-01	9.37502E-01	1.01646E-01	9.37502E-01	5.82187E-02	9.37502E-01	1.92319E-02	9.37502E-01	7.26649E-04
0.10	9.37502E-01	1.87180E-01	9.37502E-01	1.07518E-01	9.37502E-01	6.18906E-02	9.37502E-01	2.06305E-02	9.37502E-01	7.96041E-04
0.15	9.37502E-01	1.95181E-01	9.37502E-01	1.12645E-01	9.37502E-01	6.51273E-02	9.37502E-01	2.18801E-02	9.37502E-01	8.59153E-04
0.20	9.37502E-01	2.02526E-01	9.37502E-01	1.17354E-01	9.37502E-01	6.81010E-02	9.37502E-01	2.30295E-02	9.37502E-01	9.17215E-04
0.25	9.37502E-01	2.09329E-01	9.37502E-01	1.21700E-01	9.37502E-01	7.08390E-02	9.37502E-01	2.40838E-02	9.37502E-01	9.69867E-04
0.30	9.37502E-01	2.14488E-01	9.37502E-01	1.25033E-01	9.37502E-01	7.29570E-02	9.37502E-01	2.49093E-02	9.37502E-01	1.01167E-03
0.35	9.37502E-01	2.18758E-01	9.37502E-01	1.27782E-01	9.37502E-01	7.46990E-02	9.37502E-01	2.55856E-02	9.37502E-01	1.04557E-03
0.40	9.37502E-01	2.21644E-01	9.37502E-01	1.29660E-01	9.37502E-01	7.58996E-02	9.37502E-01	2.60572E-02	9.37502E-01	1.06953E-03
0.45	9.37502E-01	2.24010E-01	9.37502E-01	1.31146E-01	9.37502E-01	7.68233E-02	9.37502E-01	2.64054E-02	9.37502E-01	1.08606E-03
0.50	9.37502E-01	2.24480E-01	9.37502E-01	1.31463E-01	9.37502E-01	7.70310E-02	9.37502E-01	2.64899E-02	9.37502E-01	1.09056E-03
0.55	9.37502E-01	2.24010E-01	9.37502E-01	1.31146E-01	9.37502E-01	7.68233E-02	9.37502E-01	2.64054E-02	9.37502E-01	1.08606E-03
0.60	9.37502E-01	2.21644E-01	9.37502E-01	1.29660E-01	9.37502E-01	7.58996E-02	9.37502E-01	2.60572E-02	9.37502E-01	1.06953E-03
0.65	9.37502E-01	2.18758E-01	9.37502E-01	1.27782E-01	9.37502E-01	7.46990E-02	9.37502E-01	2.55856E-02	9.37502E-01	1.04557E-03
0.70	9.37502E-01	2.14488E-01	9.37502E-01	1.25033E-01	9.37502E-01	7.29570E-02	9.37502E-01	2.49093E-02	9.37502E-01	1.01167E-03
0.75	9.37502E-01	2.09329E-01	9.37502E-01	1.21700E-01	9.37502E-01	7.08390E-02	9.37502E-01	2.40838E-02	9.37502E-01	9.69867E-04
0.80	9.37502E-01	2.02526E-01	9.37502E-01	1.17354E-01	9.37502E-01	6.81010E-02	9.37502E-01	2.30295E-02	9.37502E-01	9.17215E-04
0.85	9.37502E-01	1.95181E-01	9.37502E-01	1.12645E-01	9.37502E-01	6.51273E-02	9.37502E-01	2.18801E-02	9.37502E-01	8.59153E-04
0.90	9.37502E-01	1.87180E-01	9.37502E-01	1.07518E-01	9.37502E-01	6.18906E-02	9.37502E-01	2.06305E-02	9.37502E-01	7.96041E-04
0.95	9.37502E-01	1.77908E-01	9.37502E-01	1.01646E-01	9.37502E-01	5.82187E-02	9.37502E-01	1.92319E-02	9.37502E-01	7.26649E-04
1.00	9.37502E-01	1.69549E-01	9.37502E-01	9.62003E-02	9.37502E-01	5.47449E-02	9.37502E-01	1.78750E-02	9.37502E-01	6.57274E-04

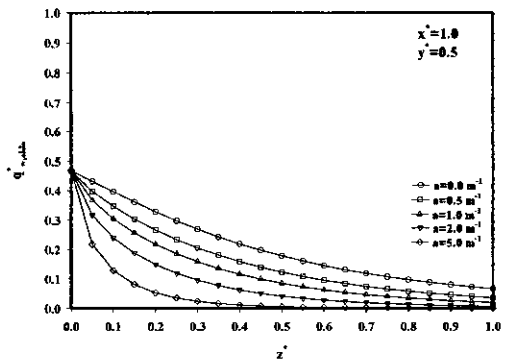

(a) Side wall heat flux

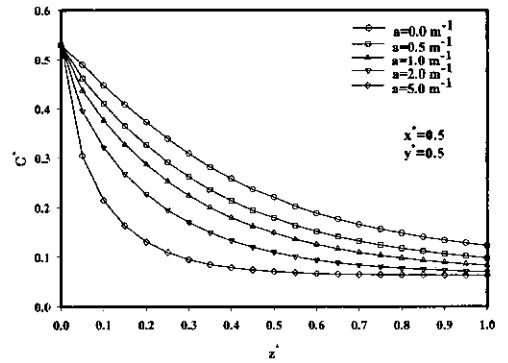

(b) Average intensity

Fig. 3 Net side wall heat flux and average intensity distributions for gray gases(T_g=0.5 T_{hot})

shows the dimensionless net wall heat flux distributions on the top cold wall for different absorption coefficients. The data show that the net wall heat flux on the top cold wall decreases as the absorption coefficient increases due to the increased optical depth. Data used for Fig. 2 are listed in Table 1.

Figure 3 shows the dimensionless side wall heat flux and average intensity distributions for different absorption coefficients. The data show that the net side wall heat flux decreases as the absorption coefficient increases. Figure 3 also shows the dimensionless average intensity distributions through the medium for different absorption coefficients. The data show that the average intensity within the medium decreases as the absorption coefficient increases. Data used for Fig. 3 are listed in Table 2. The solution listed in Table 2 indicates that the dimensionless average intensity on the hot wall at z^*=0 is 0.531250 which coincides with the exact solution, and approaches the exact solution of 0.0625 at the cold wall as the optical depth increases.

Table 2 Net side wall heat flux and average intensity distributions($T_g=0.5T_{hot}$)

z^*	a=0.0		a=0.5		a=1.0		a=2.0		a=5.0	
	$q^*_{w,side}$	G^*	$q^*_{w,side}$	G^*	$q^*_{w,side}$	G^*	$q^*_{w,side}$	G^*	$q^*_{w,side}$	G^*
0.00	4.68751E-01	5.31250E-01	4.68751E-01	5.31250E-01	4.68751E-01	5.31250E-01	4.68751E-01	5.31250E-01	4.68751E-01	5.31250E-01
0.05	4.32161E-01	4.89004E-01	3.97284E-01	4.62165E-01	3.67099E-01	4.37902E-01	3.17276E-01	3.95771E-01	2.18073E-01	3.04555E-01
0.10	3.96058E-01	4.48159E-01	3.46314E-01	4.10104E-01	3.04926E-01	3.76718E-01	2.40472E-01	3.21288E-01	1.29304E-01	2.14450E-01
0.15	3.61408E-01	4.09097E-01	3.03566E-01	3.65229E-01	2.56960E-01	3.27691E-01	1.87744E-01	2.67654E-01	8.16446E-02	1.62679E-01
0.20	3.28413E-01	3.73309E-01	2.66456E-01	3.26498E-01	2.17924E-01	2.87364E-01	1.48800E-01	2.26918E-01	5.33201E-02	1.30267E-01
0.25	2.97337E-01	3.39259E-01	2.33904E-01	2.91724E-01	1.85463E-01	2.52832E-01	1.19039E-01	1.94663E-01	3.55846E-02	1.09000E-01
0.30	2.69178E-01	3.09020E-01	2.05672E-01	2.61805E-01	1.58378E-01	2.23997E-01	9.58793E-02	1.69224E-01	2.41082E-02	9.47438E-02
0.35	2.42964E-01	2.81874E-01	1.80679E-01	2.35767E-01	1.35374E-01	1.99626E-01	7.75464E-02	1.48883E-01	1.65139E-02	8.50140E-02
0.40	2.19088E-01	2.58212E-01	1.58766E-01	2.13545E-01	1.15881E-01	1.79282E-01	6.29483E-02	1.32673E-01	1.14101E-02	7.83134E-02
0.45	1.97543E-01	2.36967E-01	1.39618E-01	1.94121E-01	9.93523E-02	1.61957E-01	5.12593E-02	1.19552E-01	7.93824E-03	7.36443E-02
0.50	1.78142E-01	2.20779E-01	1.22858E-01	1.79105E-01	8.52809E-02	1.48532E-01	4.18348E-02	1.09536E-01	5.55163E-03	7.04383E-02
0.55	1.60727E-01	2.02373E-01	1.08250E-01	1.63342E-01	7.33507E-02	1.35295E-01	3.42549E-02	1.00574E-01	3.90501E-03	6.81011E-02
0.60	1.45237E-01	1.88378E-01	9.55258E-02	1.51200E-01	6.31929E-02	1.25074E-01	2.81057E-02	9.37461E-02	2.75711E-03	6.64900E-02
0.65	1.31152E-01	1.76234E-01	8.42975E-02	1.40820E-01	5.44747E-02	1.16489E-01	2.30979E-02	8.82334E-02	1.95381E-03	6.53518E-02
0.70	1.18587E-01	1.65333E-01	7.44863E-02	1.31708E-01	4.70241E-02	1.09122E-01	1.90141E-02	8.37158E-02	1.38862E-03	6.45415E-02
0.75	1.07343E-01	1.55899E-01	6.59067E-02	1.23922E-01	4.06583E-02	1.02927E-01	1.56849E-02	8.00576E-02	9.90037E-04	6.39661E-02
0.80	9.73975E-02	1.47664E-01	5.84515E-02	1.17215E-01	3.52357E-02	9.76799E-02	1.29695E-02	7.70776E-02	7.07963E-04	6.35557E-02
0.85	8.83429E-02	1.40053E-01	5.18321E-02	1.11186E-01	3.05383E-02	9.30856E-02	1.07294E-02	7.45964E-02	5.07070E-04	6.32604E-02
0.90	8.02553E-02	1.33495E-01	4.60361E-02	1.06042E-01	2.65112E-02	8.92214E-02	8.89238E-03	7.25831E-02	3.64070E-04	6.30497E-02
0.95	7.33702E-02	1.27852E-01	4.11248E-02	1.01643E-01	2.31371E-02	8.59589E-02	7.40312E-03	7.09410E-02	2.62250E-04	6.28986E-02
1.00	6.61485E-02	1.22585E-01	3.62967E-02	9.76524E-02	1.99838E-02	8.30769E-02	6.11741E-03	6.95622E-02	1.88567E-04	6.27891E-02

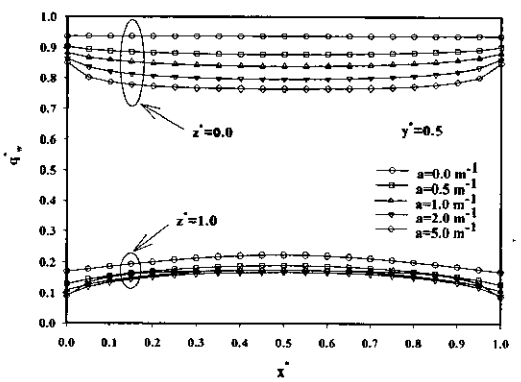

Fig. 4 Net wall heat fluxes for gray gases($T_g=0.5T_{hot}$)

3.1.2 Intermediate gray gas temperature

Now consider a black walled cubical enclosure where the bottom black wall is maintained at $T_{hot}=1000K$, all the other black walls are maintained at $T_{cold}=0.5T_{hot}$ and the medium is maintained at intermediate temperature of 0.7 T_{hot}. This problem is solved by using the discrete transfer method using the T_{95} quadrature set which was proved to result in accurate solutions in the previous section.

Figure 4 shows the dimensionless net wall heat flux distributions on the bottom hot wall and top cold wall respectively for different absorption coefficients. In Fig. 4 the nonparticipating medium of $a=0.0$ results in a constant hot wall radiative heat flux of 0.937502 which agrees well with the exact solution of 0.9375, and the net hot wall radiative heat flux decreases as the absorption coefficient increases. Figure 4 also shows the net radiative heat fluxes on the top cold wall for different absorption coefficients. The cold wall heat flux decreases as optical depth increases for small optical depths, but the trend is reversed as the medium optical depth increases further, which is due to the increased effect of emission from the hot medium at 0.7 T_{hot}. We may expect that the net cold wall heat flux approaches the exact value of 0.1776(radiative exchange between 0.7 T_{hot} and 0.5
T_{hot}) as the medium optical depth increases further.

Figure 5 shows the dimensionless net side wall radiative flux and the average intensity distributions through the medium for different

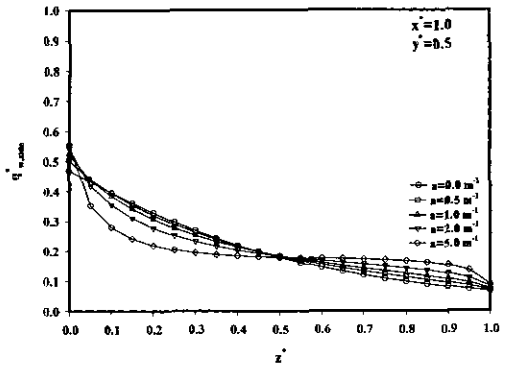

(a) Side wall heat flux

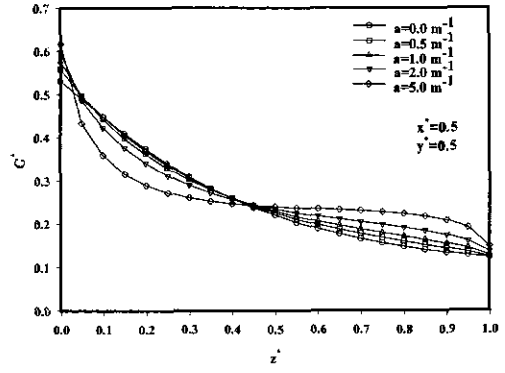

(b) Average intensity

Fig. 5 Net side wall heat flux and average intensity distributions for gray gases($T_g=0.7\,T_{hot}$)

absorption coefficients. The data show that the net side wall radiative flux increases near the hot wall, decreases at closer locations from the hot wall and increases again near the cold wall as the absorption coefficient increases. This is due to the increased effect of the medium emission. Figure 5 shows that the dimensionless net side wall radiative flux near the mid point on the side wall approaches the exact solution of 0.1776 as the optical depth increases. Figure 5 also shows the dimensionless average intensity distributions through the medium for different absorption coefficients. The data show that the dimensionless average intensity increases near the hot wall, decreases at closer locations from the hot wall and increases again near the cold wall as the absorption coefficient increases, which is the same trend as the side wall radiative heat flux distribution. By examining the average intensity distributions, we expect the dimensionless average intensity near the mid point within the medium approaches the exact value of 0.2401 for very large optical depths.

3.2 Nongray gas solutions

For nongray uniform gases, Eq. (4) can be used. The exponential term is defined as the transmittance $\tau_\lambda(\Delta s)$ of the medium and is expressed by

$$\tau_\lambda(\Delta s)=e^{-a_\lambda \Delta s} \tag{13}$$

where $\Delta S=s_p-s_u$ is the path length. Then Eq. (4) is expressed in a simpler form as

$$I_{\lambda,p}(s_p,\ \Omega)=I_{\lambda,u}(s_u,\ \Omega)\tau_\lambda(\Delta s)+I_{\lambda b}[1-\tau_\lambda(\Delta S)] \tag{14}$$

If the upstream point u is on a black surface, such as $I_{\lambda,u}=I_{\lambda bw}$, then Eq. (14) becomes

$$I_{\lambda,\ p}(s_p,\ \Omega)=I_{\lambda bw}\tau_\lambda(\Delta s)+I_{\lambda b}[1-\tau_\lambda(\Delta s)] \tag{15}$$

If we want to apply a band approximation such as the narrow band model, spectral average of Eq. (15) over a bandwidth $\Delta\lambda$ is needed.

$$\frac{1}{\Delta\lambda}\int_{\lambda_L}^{\lambda_U} I_{\lambda,p}(s,\ \Omega)d\lambda=\frac{1}{\Delta\lambda}\int_{\lambda_L}^{\lambda_U} I_{\lambda bw}\tau_\lambda(\Delta s)d\lambda + \frac{1}{\Delta\lambda}\int_{\lambda_L}^{\lambda_U} I_{\lambda b}d\lambda-\frac{1}{\Delta\lambda}\int_{\lambda_L}^{\lambda_U} I_{\lambda b}\tau_\lambda(\Delta s)d\lambda \tag{16}$$

Where the narrow band has the lower limit $\lambda_L=\lambda-\Delta\lambda/2$ and the upper limit $\lambda_U=\lambda+\Delta\lambda/2$.

Since the spectral dependency of the transmittance is very strong for most of the gases, we have to be careful in dealing with the spectral correlations between the transmittance and other variables (Zhang, Soufiani, and Taine, 1988). The first and the last terms on the right hand side of Eq. (16) have this kind of spectral correlations. However, since the spectral variation of the blackbody intensity is relatively smooth as compared to the transmittance, the spectral correlation between the blackbody intensity and the transmittance is negligible (Zhang, Soufiani, and Taine, 1988; Soufiani and Taine, 1989; Kim, Menart and Lee, 1991). Then Eq. (16) can be approximated as

$$\frac{1}{\Delta\lambda}\int_{\lambda_L}^{\lambda_U} I_{\lambda,p}(s,\ \Omega)d\lambda$$
$$\fallingdotseq \frac{\sigma T_w^4}{\Delta\lambda}\left[\int_{\lambda_L}^{\lambda_U}\frac{I_{\lambda bw}}{\sigma T_w^4}d\lambda\right]\left[\frac{1}{\Delta\lambda}\int_{\lambda_L}^{\lambda_U}\tau_\lambda(\Delta s)d\lambda\right]$$
$$+\frac{\sigma T_g^4}{\Delta\lambda}\left[\int_{\lambda_L}^{\lambda_U}\frac{I_{\lambda b}}{\sigma T_g^4}d\lambda\right]-\frac{\sigma T_g^4}{\Delta\lambda}\left[\int_{\lambda_L}^{\lambda_U}\frac{I_{\lambda b}}{\sigma T_g^4}d\lambda\right]$$
$$\left[\frac{1}{\Delta\lambda}\int_{\lambda_L}^{\lambda_U}\tau_\lambda(\Delta_s)d\lambda\right] \tag{17a}$$

or

$$\overline{I}_{\lambda,p}(s_p)=\frac{\sigma T_g^4}{\pi\Delta\lambda}F_{T_g\lambda_L-T_g\lambda_U}$$
$$+\sigma[\,T_w^4 F_{T_w\lambda_L-T_w\lambda_U}-T_g^4 F_{T_g\lambda_L-T_g\lambda_U}]\frac{\overline{\tau}_\lambda(\Delta s)}{\tau\Delta\lambda} \tag{17b}$$

where the band average intensity $\overline{I}_{\lambda,p}$, the band average transmittance $\overline{\tau}_\lambda$, and the blackbody fraction over the band $F_{T_g\lambda_L-T_g\lambda^U}$ are defined as

$$\overline{I}_{\lambda,p}(s_p)=\frac{1}{\Delta\lambda}\int_{\lambda_L}^{\lambda_U} I_{\lambda,p}(s,\ \Omega)d\lambda \tag{18}$$

$$\overline{\tau}_\lambda=\frac{1}{\Delta\lambda}\int_{\lambda_L}^{\lambda_U}\tau_\lambda(\Delta s)d\lambda \tag{19}$$

$$F_{T_g\lambda_L-T_g\lambda_U}=\int_{\lambda_L}^{\lambda_U}\frac{\pi I_{\lambda b}}{\sigma T_g^4}d\lambda \tag{20}$$

where the average transmittance for each narrow band is computed by using the statistical narrow band model (Ludwig, Malkmus, Readon, and Thompson, 1973).

For a discrete direction Ω_m as shown in Fig. 1 and for a narrow band at λ_k, Eq. (17b) can be expressed in the following discrete form.

$$\overline{I}_{k,p,m}=\frac{\sigma T_g^4}{\pi\Delta\lambda_k}F_{T_g\lambda_{k,L}-T_g\lambda_{k,U}}$$
$$+\sigma[\,T_w^4 F_{T_w\lambda_{k,L}-T_w\lambda_{k,U}}$$
$$-T_g^4 F_{T_g\lambda_{k,L}-T_g\lambda_{k,U}}]\frac{\overline{\tau}_k(\Delta s_m)}{\tau\Delta\lambda_k} \tag{21}$$

where $\Delta\lambda_k$ is the width of the k^{th} band.

Once the band average intensities for all K bands are obtained, the total intensity at point p is computed as

$$I_{p,m}=\sum_{k=1}^{K}\overline{I}_{k,p,m}\Delta\lambda_k \tag{22}$$

where K is the total number of narrow bands considered. A sufficiently wide range of the wave number between 50 and 10,000cm^{-1}, which results in about 0.0111% relative error for the total black body intensity at 500K, is considered for all the spectral integrations.

The total radiative wall heat flux q_w and the total average intensity G can be estimated as in Eqs. (7) and (8) by using the total intensity $I_{p,m}$ shown in Eq. (22).

3.2.1 Simple nongray gas system

As an ultimate case, if the bottom black wall is maintained at $T_{hot}=1000K$ and all other black walls and the medium are maintained cold at $T_g=T_{cold}=0.5T_{hot}$, the total radiative intensity for all incident directions into the bottom wall is simply $I_{p,m}=\sigma T_{cold}^4/\pi$ for $|\Omega_m\cdot\hat{n}|<0$ b y examining Eqs. (21) and (22), which is the same result as the gray gas problem discussed in section 3.1.1 Therefore, the total net radiative heat flux and the total average intensity on the hot wall in a dimensionless form are expressed as the Eqs. (10) and (12), respectively. For $T_{hot}=1000K$ and $T_{cold}=0.5T_{hot}$, the exact nongray gas solutions of $(q^*_{w,hot})_{exact}=0.9375$ and $(G^*_{w,hot})_{exact}=0.53125$ on the hot wall can be obtained.

The same nongray gas problem is solved by using the statistical narrow band model and the discrete transfer method with the T_{95} quadrature set. The typical c.p.u. time spent for the nongray gas solution(21 points on the bottom, top, side and in the medium respectively) by using the T_{95} quadrature set is about 11 hours for pure H_2O and about 30 hours for CO_2 mixtures on a Pentium II 400MHz PC.

Figure 6 shows the constant dimensionless total net hot wall heat fluxes of 0.937516 for pure H_2O and 0.937509 for CO_2 mixtures which are quite accurate as compared to the exact solution of 0. 9375 with the percent relative errors of 0. 0017067% and 0.00096%, respectively. Figure 6 also shows the dimensionless total net wall heat flux distributions on the top cold wall for various mixture gases of H_2O and CO_2 by maintaining the total pressure at 1 atm. The data show that the net wall heat flux on the top cold wall decreases with the CO_2 mole fraction which says that the CO_2 gas absorbs less radiative energy as compared to the H_2O gas. Data used for Fig. 6 are listed in Table 3.

Figure 7 shows the dimensionless total net side

Table 3 Net hot and cold wall heat fluxes for nongray gases($T_g=0.5T_{hot}$)

x^*	Pure H_2O		Pure CO_2		$0.5H_2O+0.5CO_2$		$0.2H_2O+0.8CO_2$	
	$q^*_{w,hot}$	$q^*_{w,cold}$	$q^*_{w,hot}$	$q^*_{w,cold}$	$q^*_{w,hot}$	$q^*_{w,cold}$	$q^*_{w,hot}$	$q^*_{w,cold}$
0.00	9.37516E-01	1.04261E-01	9.37509E-01	1.48269E-01	9.37509E-01	1.06499E-01	9.37509E-01	1.20501E-01
0.05	9.37516E-01	1.09596E-01	9.37509E-01	1.55615E-01	9.37509E-01	1.11947E-01	9.37509E-01	1.26615E-01
0.10	9.37516E-01	1.15467E-01	9.37509E-01	1.63754E-01	9.37509E-01	1.17943E-01	9.37509E-01	1.33355E-01
0.15	9.37516E-01	1.20551E-01	9.37509E-01	1.70781E-01	9.37509E-01	1.23135E-01	9.37509E-01	1.39187E-01
0.20	9.37516E-01	1.25218E-01	9.37509E-01	1.77232E-01	9.37509E-01	1.27901E-01	9.37509E-01	1.44540E-01
0.25	9.37516E-01	1.29536E-01	9.37509E-01	1.83206E-01	9.37509E-01	1.32311E-01	9.37509E-01	1.49495E-01
0.30	9.37516E-01	1.32822E-01	9.37509E-01	1.87738E-01	9.37509E-01	1.35666E-01	9.37509E-01	1.53262E-01
0.35	9.37516E-01	1.35538E-01	9.37509E-01	1.91488E-01	9.37509E-01	1.38440E-01	9.37509E-01	1.56377E-01
0.40	9.37516E-01	1.37664E-01	9.37509E-01	1.94428E-01	9.37509E-01	1.40612E-01	9.37509E-01	1.58816E-01
0.45	9.37516E-01	1.38874E-01	9.37509E-01	1.96101E-01	9.37509E-01	1.41848E-01	9.37509E-01	1.60204E-01
0.50	9.37516E-01	1.39177E-01	9.37509E-01	1.96514E-01	9.37509E-01	1.42157E-01	9.37509E-01	1.60550E-01
0.55	9.37516E-01	1.38874E-01	9.37509E-01	1.96101E-01	9.37509E-01	1.41848E-01	9.37509E-01	1.60204E-01
0.60	9.37516E-01	1.37379E-01	9.37509E-01	1.94024E-01	9.37509E-01	1.40321E-01	9.37509E-01	1.58487E-01
0.65	9.37516E-01	1.35538E-01	9.37509E-01	1.91488E-01	9.37509E-01	1.38440E-01	9.37509E-01	1.56377E-01
0.70	9.37516E-01	1.32822E-01	9.37509E-01	1.87738E-01	9.37509E-01	1.35666E-01	9.37509E-01	1.53262E-01
0.75	9.37516E-01	1.29536E-01	9.37509E-01	1.83206E-01	9.37509E-01	1.32311E-01	9.37509E-01	1.49495E-01
0.80	9.37516E-01	1.25218E-01	9.37509E-01	1.77232E-01	9.37509E-01	1.27901E-01	9.37509E-01	1.44540E-01
0.85	9.37516E-01	1.20551E-01	9.37509E-01	1.70781E-01	9.37509E-01	1.23135E-01	9.37509E-01	1.39187E-01
0.90	9.37516E-01	1.15341E-01	9.37509E-01	1.63577E-01	9.37509E-01	1.17815E-01	9.37509E-01	1.33210E-01
0.95	9.37516E-01	1.09596E-01	9.37509E-01	1.55615E-01	9.37509E-01	1.11947E-01	9.37509E-01	1.26615E-01
1.00	9.37516E-01	1.04261E-01	9.37509E-01	1.48269E-01	9.37509E-01	1.06499E-01	9.37509E-01	1.20501E-01

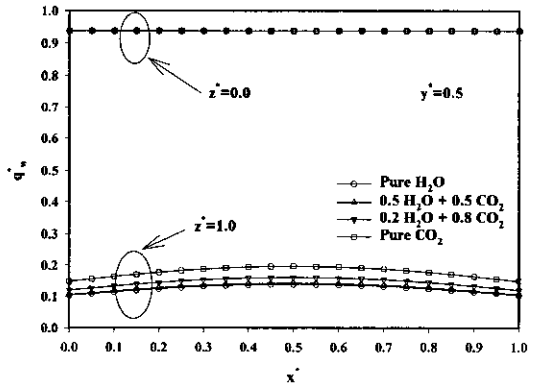

Fig. 6 Net wall heat fluxes for nongray gases($T_g=0.5T_{hot}$)

wall heat fluxes for the same conditions. The data show that the net wall heat flux on the side wall also decreases with the CO_2 mole fraction. Figure 7 also shows the dimensionless average intensity distributions through the medium for various mixture gases of H_2O and CO_2, and the average intensity within the medium decreases with the CO_2 mole fraction. Data shown in Fig. 7 are listed in Table 4.

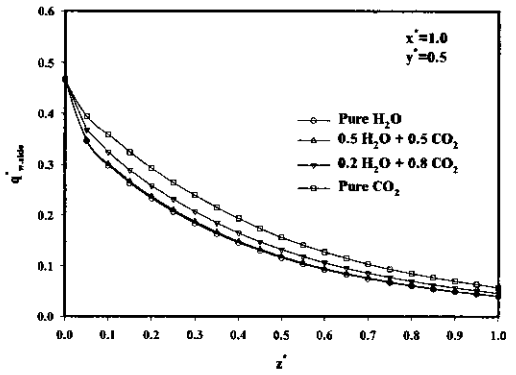

(a) Side wall heat flux

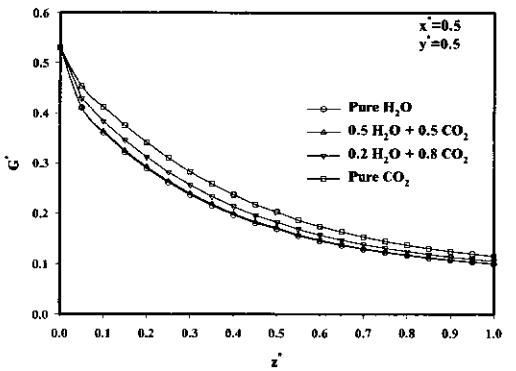

(b) Average intensity

Fig. 7 Net side wall heat flux and average intensity distributions for nongray gases($T_g=0.5T_{hot}$)

Table 4 Net side wall heat flux and average intensity distributions for nongray gases($T_g=0.5T_{hot}$)

x^*	Pure H_2O		Pure CO_2		$0.5H_2O+0.5CO_2$		$0.2H_2O+0.8CO_2$	
	$q^*_{w,hot}$	$q^*_{w,cold}$	$q^*_{w,hot}$	$q^*_{w,cold}$	$q^*_{w,hot}$	$q^*_{w,cold}$	$q^*_{w,hot}$	$q^*_{w,cold}$
0.00	4.68730E-01	5.31229E-01	4.68747E-01	5.31246E-01	4.68747E-01	5.31246E-01	4.68747E-01	5.31246E-01
0.05	3.45336E-01	4.10528E-01	3.94069E-01	4.53024E-01	3.46629E-01	4.11072E-01	3.66650E-01	4.29195E-01
0.10	2.98623E-01	3.60494E-01	3.57157E-01	4.11794E-01	3.01679E-01	3.62906E-01	3.24103E-01	3.83205E-01
0.15	2.63084E-01	3.21551E-01	3.23913E-01	3.74509E-01	2.66667E-01	3.24572E-01	2.89168E-01	3.44775E-01
0.20	2.33140E-01	2.89234E-01	2.93123E-01	3.41119E-01	2.36801E-01	2.92400E-01	2.58482E-01	3.11718E-01
0.25	2.07016E-01	2.60608E-01	2.64570E-01	3.09816E-01	2.10558E-01	2.63690E-01	2.31005E-01	2.81684E-01
0.30	1.84399E-01	2.36160E-01	2.38922E-01	2.82230E-01	1.87740E-01	2.39069E-01	2.06836E-01	2.55668E-01
0.35	1.64178E-01	2.14901E-01	2.15215E-01	2.57611E-01	1.67275E-01	2.17594E-01	1.84940E-01	2.32789E-01
0.40	1.46280E-01	1.96767E-01	1.93729E-01	2.36236E-01	1.49124E-01	1.99238E-01	1.65376E-01	2.13121E-01
0.45	1.30485E-01	1.80837E-01	1.74410E-01	2.17115E-01	1.33080E-01	1.83085E-01	1.47986E-01	1.95716E-01
0.50	1.16520E-01	1.68684E-01	1.57066E-01	2.02546E-01	1.18879E-01	1.70755E-01	1.32520E-01	1.82429E-01
0.55	1.04192E-01	1.55457E-01	1.41536E-01	1.86094E-01	1.06332E-01	1.57306E-01	1.18797E-01	1.67780E-01
0.60	9.33595E-02	1.45379E-01	1.27749E-01	1.73582E-01	9.52985E-02	1.47055E-01	1.06692E-01	1.56616E-01
0.65	8.36509E-02	1.36724E-01	1.15239E-01	1.62743E-01	8.54042E-02	1.38246E-01	9.57965E-02	1.46996E-01
0.70	7.50782E-02	1.29051E-01	1.04096E-01	1.53031E-01	7.66635E-02	1.30432E-01	8.61465E-02	1.38436E-01
0.75	6.74848E-02	1.22463E-01	9.41380E-02	1.44637E-01	6.89184E-02	1.23720E-01	7.75733E-02	1.31066E-01
0.80	6.08219E-02	1.16757E-01	8.53407E-02	1.37317E-01	6.21203E-02	1.17903E-01	7.00331E-02	1.24667E-01
0.85	5.48153E-02	1.11549E-01	7.73422E-02	1.30565E-01	5.59902E-02	1.12592E-01	6.32172E-02	1.18806E-01
0.90	4.94916E-02	1.07087E-01	7.02056E-02	1.24751E-01	5.05559E-02	1.08040E-01	5.71631E-02	1.13775E-01
0.95	4.49720E-02	1.03262E-01	6.41324E-02	1.19751E-01	4.59415E-02	1.04137E-01	5.20184E-02	1.09457E-01
1.00	4.03263E-02	9.97326E-02	5.77795E-02	1.15093E-01	4.11975E-02	1.00535E-01	4.67046E-02	1.05460E-01

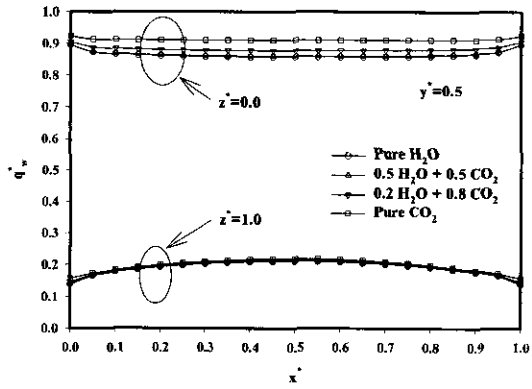

Fig. 8 Net wall heat fluxes for nongray gases($T_g=0.7T_{hot}$)

3.2.2 Intermediate nongray gas temperature

Now consider a black walled cubical enclosure where the bottom black wall is maintained at $T_{hot}=1000K$, all other black walls are maintained at $T_{cold}=0.5T_{hot}$ and the medium is maintained at intermediate temperature of $0.7T_{hot}$. The nongray gas problem is solved by using the statistical narrow band model and the discrete transfer method with the T_{95} quadrature set which was proved to result in accurate solutions in the previous section.

Figure 8 shows the dimensionless net wall heat flux distributions on the bottom hot wall and top cold wall respectively for various mixture gases of H_2O and CO_2 at 1 atm. The figure shows that the net wall heat flux on the bottom hot wall decreases as the CO_2 mole fraction decreases. Figure 8 also shows the dimensionless total net wall heat flux distributions on the top cold wall for various mixture gases of H_2O and CO_2. The net wall heat flux on the top cold wall increases as the CO_2 mole fraction decreases.

Figure 9 shows the dimensionless total net side wall heat flux and the average intensity distributions for the same conditions. The data show that the net wall heat flux on the side wall increases as the CO_2 mole fraction decreases, and the side wall heat flux decreases rapidly near the top cold wall due to the lower cold wall temperature. Figure 9 also shows the dimensionless average intensity distributions through the medium for different CO_2 mole fractions. The average intensity within the medium decreases with the CO_2 mole fraction, and the average intensity decreases rapidly near the top cold wall since the

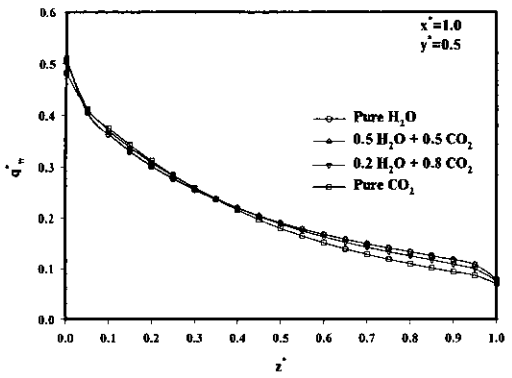

(a) Side wall heat flux

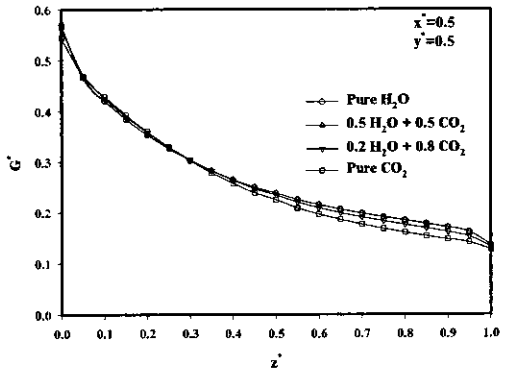

(b) Average intensity

Fig. 9 Net side wall heat flux and average intensity distributions for nongray gases($T_g=0.7\,T_{hot}$)

top wall is in lower temperature than the medium.

4. Conclusions

Exact benchmark solutions for the radiative transfer within three dimensional enclosures are very rare and many researchers have difficulty in evaluating their solutions obtained from the multidimensional systems using various solution schemes suitable for engineering purposes. In this paper we present some benchmark solutions for purely absorbing gray and nongray gases including the H_2O and CO_2 by using the discrete transfer method with sufficiently accurate T_{95} quadrature set. Analytically obtained exact solutions at various conditions are used to check the solutions obtained from the numerical method, and we found that the numerical solutions obtained from this study were very well matched with the available exact values. The trends of the solutions are also found to be physically reasonable for different absorption coefficients. The nongray real gas solutions for mixtures of H_2O and CO_2 are also obtained for the same conditions as the gray gases, and the results may be used as the benchmark solutions in developing the solution schemes for nongray gas radiation. The typical relative percent errors observed for the data presented in this paper are about 0.0002% for the gray gas solutions and about 0.001% for the nongray gas solutions as compared to the exact solutions available.

Acknowledgements

The authors wish to acknowledge the financial supports of the RACER and the CERC.

References

Carlson, B.G. and Lathrop, K.D., 1968, "Transport Theory-The Method of Discrete Ordinates ," *Computing Methods in Reactor Physics*, Greenspan, H., Kelber, C.N., and Okrent, D. eds., Gordon and breach, New York.

Cha, H.J. and Song, T.H., 1999, "Discrete Ordinates Interpolation Method applied to Irregular Three-Dimensional Geometries," *Proceedings of the KSME 1999 Fall Annual Meeting in Heat Engineering Division*, pp 365~372

Chai, J.C., Lee, H.S. and Patankar, S. V., 1994, "Treatment of Irregular Geometries Using a Cartesian Coordinates Finite-Volume Radiation Heat Transfer Procedure," *Numerical Heat Transfer*, Part B, Vol. 26., pp. 225~235.

Cheong, K.B. and Song, T.H. 1997, "Discrete Ordinates Interpolation Method for Numerical Solution of Two-Dimensional Radiative Transfer Problems," *Numercial Heat Transfer*, Part B, Vol. 32, pp. 107~125.

Fiveland, W.A., 1984, "Discrete-Ordinates Solutions of the Radiative Transport Equation for Rectangular Enclosures," *ASME Journal of Heat Transfer*, Vol. 106, pp. 699~706.

Grosshandler, W. L., 1980, "Radiative Transfer in Nonhomogeneous Gases : A Simplified Ap-

proach," *Int. J. Heat and Mass Transfer*, Vol. 23, pp. 1447~1459.

Hottel, H. C. and Sarofim, A. F., 1967, *Radiative Transfer*, McGraw-Hill.

Howell, J.R. and Perlmutter, M., 1964, "Monte Carlo Solution of Thermal Transfer through Radiant Media Between Gray Walls," ASME Journal of Heat Transfer, Vol. 86, No. 1, pp. 116~122.

Kim, T.K. and Lee, H., 1988 "Effect of Anisotropic Scattering on Radiative Heat Transfer in Two-Dimensional Rectangular Enclosures," *Int. J. of Heat and Mass Transfer*, Vol. 31, No. 8, pp. 1711~1721.

Kim, T.K., Menart, J.A. and Lee, H., 1991, "Nongray Radiative Gas Analyses Using the S-N Technique," *ASME J. of Heat Transfer*, Vol. 113, pp. 946~952.

Kim, T.K., Seo, S.H., Min, D.H. and Son, B. S., 1998, "Study on Radiation in 3-D Irregular Systems Using the Trapezoidal Rule Approximation on the Transport Equation," *KSME international Journal*, Vol. 12, No. 3, pp. 514~523.

Lockwood, F. C. and Shah, N. G., 1981, "A New Radiation Solution Method for Incorporation in General Combustion Predictions Procedure," *in 18th Symposium on Combustion, The Combustion Institute, Pittsburg*, PA, pp. 1405~1414.

Lockwood, F.C. and Spalding, D.B., 1997, "Prediction of a Turbulent Duct Flow with Significant Radiation," *Proc. Thermodynamics Colloquium.*

Ludwig, C.B., Malkmus, W., Readon, J.E. and Thompson, A.L., 1973, *Handbook of Infrared Radiation from Combustion Gases*, NASA SP-3080, Scientific and Technical Information Office, Washington D.C..

Menguc, M.P. and Viskanta, R., 1985, "Radiative Transfer In Three-Dimensional Rectangular Enclosures Containing Inhomogeneous, Anisotropically Scattering Media" *J. of Quant. Spectro. and Radiative Trans.*, Vol. 33, No. 6, pp. 533~549.

Modest, M. F., 1993, *Radiative Heat Transfer*, McGraw-Hill, Inc..

Raithby, G.D. and Chui, E. H., 1990, "A Finite-Volume Method for Predicting a Radiant Heat Transfer in Enclosure with Participating Media," *ASME J. Heat Transfer*, Vol. 112, pp. 415~423.

Siegel, R., 1991, "Analytical Solution for Boundary Heat Fluxes From a Radiating -ectangular Medium," *J. Heat Transfer*, Vol. 113, pp. 258~261

Siegel, R., 1992, "Boundary Fluxes for Spectral Radiation From Uniform Temperature Rectangular Enclosures," *J. Heat Transfer*, Vol. 6, pp. 543~546

Siegel, R. and Howell, J. R., 1992, *Thermal Radiation Heat Transfer*, McGraw-Hill Book Co., 3nd Ed.

Soufiani, A. and Taine, J., 1989, "Experimental and Theoretical Studies of Combined Iadiative and Convective Transfer in CO_2 and H_2O Laminar Flows," *Int. J. of Heat and Mass Transfer*, Vol. 32, No. 3, pp. 447~486.

Thurgood, C. P., Pollard, A. and Becker, H. A., 1995 "The T_N Quadrature Set for the Discrete Ordinates Method," *ASME J. of Heat Transfer*, Vol. 117, pp. 1068~1070.

Seo, S.H. and Kim, T.K., 1998, "Study on Interpolation Schemes of the Discrete Ordinates Interpolation Method for 3-D Radiative Transfer with Nonorthogonal Grids," *ASME J. of Heat Transfer*, Vol. 120, pp. 1091~1094.

Zhang, L., Soufiani, A. and Taine, J., 1988, "Spectral Correlated and Noncorrelated Radiative Transfer in a Finite Axisymmetric System Containing an Absorbing and Emitting Real Gas-Particle Mixture," *Int. J. of Heat and Mass Transfer*, Vol. 18, pp. 2261~2272.